Rock Mechanics and Rock Engineering (2023) 56:4043–4059
https://doi.org/10.1007/s00603-023-03264-9

ORIGINAL PAPER

A Nodal-Based 3D Discontinuous Deformation Analysis Method with Contact Potential for Discrete Rock Block System

Yongtao Yang[1,5] · Wenan Wu[2] · Dongdong Xu[3] · Yang Xia[1,5] · Diansen Yang[4]

Received: 24 October 2022 / Accepted: 6 February 2023 / Published online: 2 March 2023

Abstract

To analyze the movement of discrete rock block systems, a nodal-based three-dimensional discontinuous deformation analysis method with contact potential (3D-NDDACP) is proposed. In the proposed 3D-NDDACP method, tetrahedral FE meshes which can be effectively generated with existing mesh generator are adopted to discretize rock blocks to better capture their deformation. Additionally, the contact potential is incorporated to treat the contact between two adjacent blocks. The introduction of contact potential significantly simplifies the implementation of the proposed 3D-NDDACP method, since the contact force can be directly computed without distinguishing contact types between any two adjacent blocks. However, in the traditional 3D-DDA method it is essential to conduct contact type judgment before computing contact forces. Note that contact type judgment is not a trivial task for 3D problems, since many different contact types including point-to-point contact, point-to-edge contact, point-to-face contact and edge-to-edge contact are involved. With the proposed 3D-NDDACP method, three benchmark problems about the movement of rock block systems are investigated. Numerical results obtained with the proposed 3D-NDDACP method are in good agreement with the theoretical solution, which means that the proposed 3D-NDDACP method can reliably and correctly simulate the movement of rock block systems. The proposed 3D-NDDACP method warrants further investigation.

Highlights

- A nodal-based 3D DDA model is proposed for modeling the discrete rock block system.
- Contact forces are computed effectively using contact volumes, without the cumbersome contact type determination.
- Simplest and most versatile tetrahedral meshes are always available for the proposed model.

Keywords Discontinuous deformation analysis method · 3D-NDDACP method · Rock block system

✉ Wenan Wu
wuwenan17@mails.ucas.edu.cn

[1] State Key Laboratory of Geomechanics and Geotechnical Engineering, Institute of Rock and Soil Mechanics, Chinese Academy of Sciences, Wuhan 430071, China

[2] Key Laboratory of Urban Security and Disaster Engineering, Ministry of Education, Beijing University of Technology, Beijing 100124, China

[3] Key Laboratory of Geotechnical Mechanics and Engineering of Ministry of Water Resources, Changjiang River Scientific Research Institute, Wuhan 430010, China

[4] The Key Laboratory of Safety for Geotechnical and Structural Engineering of Hubei Province, School of Civil Engineering, Wuhan University, Wuhan 430072, China

[5] University of Chinese Academy of Sciences, Beijing 100049, People's Republic of China

1 Introduction

Due to the long-term geological process, natural rock masses may contain a large number of structural planes (joints, faults, and weak side), and show a strong discontinuous deformation characteristic (Yang et al. 2018a, 2021a). How to accurately obtain the mechanical behavior of discontinuous rock masses has always been an attractive topic in rock mechanics. Considering economy and flexibility, numerical methods have become an effective tool to fulfil this task, such as the continuous-based methods and discontinues-based methods (Jing 2003).

Some typical continuous-based methods are the finite element method (FEM) (Zienkiewicz and Taylor 2000), the meshfree method (Rabczuk and Belytschko 2004; Zhuang et al. 2012) and the boundary element method (BEM). In continuous-based methods, discontinuity elements (Goodman 1976) are usually introduced to model the mechanical behavior of fractured rock masses (Beyabanaki et al. 2009). However, the number of discontinuity elements is usually limited, since these discontinuity elements may induce the numerical instability problem. In addition, it is difficult to model large-scale slipping and opening with discontinuity elements.

Compared to continuous-based methods, the discontinues-based methods are more suitable for discontinuity modeling, since they can directly simulate large-scale slipping and opening of rock masses. This is because in the discontinues-based methods, the problem domain is discretized into a series of individual blocks, and the motion and deformation of each block are treated separately. Furthermore, the interaction between blocks is treated using mutual contacts. Some typical discontinues-based methods are the distinct element method (DEM) (Jing 2003) introduced by Cundall, the discontinuous deformation analysis (DDA) method developed by Shi (1988) and the discrete finite element or the combined FEM-DEM developed by Munjiza (2004).

As a typical discontinuum-based method, the DDA method was originally developed to model the deformation and movement of a rock block system (Shi 1988). The DDA method can be considered as an implicit version of DEM since the contact and deformation of blocks are all included in a unified system equilibrium equation. It has been shown in many existing literature (Jing 2003; Shi 1988) that the solution of large deformation and displacement of a rock block system can be effectively solved by performing static or dynamic DDA analyses. Due to the attractive advantages of the DDA method, it has been used by researchers and engineers to solve many types of practical problems, such as dam deformation problems (Kottenstette 1999), Tunnel stability problems (Tsesarsky and Hatzor 2006), slope failure problems (Wu 2007; Yang et al. 2019, 2020a, b, 2023; Feng et al. 2021), jointed rock masses problems (Lin et al. 1996), hydraulic fracturing problems (Yang et al. 2018b; Wu et al. 2022; Choo et al. 2016) and wave propagation problems in rock masses (Wu et al. 2020a, b; Bao et al. 2012; Jiao et al. 2007; Gu and Zhao 2009). A review article about the validation of the DDA method for engineering problems can be found in (MacLaughlin and Doolin 2006). However, most of the research results mentioned above were obtained using a two-dimensional DDA (2D-DDA) method.

Note that all the practical engineering problems are in 3D space. Hence, the development of a 3D-DDA method for engineering problems is essential. Some early published work about the 3D-DDA method can be found in (Beyabanaki et al. 2008; Jiang and Yeung 2004; Yeung et al. 2003). In contrast to the 2D-DDA method, the application of the 3D-DDA method to engineering problems is not fruitful. One main reason lies behind is that contact treatment in the 3D-DDA method has not been well resolved. Compared to the 2D-DDA method, contact type judgment in the 3D-DDA method is not a trivial task, since more complex contact types, such as point-to-point contact, point-to-edge contact, point-to-face contact, edge-to-edge contact and force-to-face contact, are involved. In a typical contact-type judgment process, a rough search is first conducted to obtain the blocks closing to each other. Then, the possible contact type between adjacent blocks is determined using a fine search scheme. The contact judgment in the 3D-DDA method faces three main difficulties, namely, low efficiency, the uncertain direction of contact force and difficulty in handling concave blocks (Wang et al. 2021; Yeung et al. 2007). In addition, the first-order displacement function is used in the traditional 3D-DDA method to model the deformation of rock blocks (Yang et al. 2021b; Yeung et al. 2004). Hence, the stress and strain within any rock block computed by the traditional 3D-DDA method are constants. For a small rock block, this scheme may be acceptable. But for a big rock block in which the distributions of strain and stress are severely uneven, this approach is obviously unacceptable. To deal with the above-mentioned problems, some remedy schemes have been proposed in the past years, see for example (Wang et al. 2021; Beyabanaki et al. 2009; Zhang et al. 2016).

In the present work, to better analyze rock mechanics problems, a nodal-based 3D discontinuous deformation analysis method with contact potential (3D-NDDACP) is proposed. The proposed 3D-NDDACP method inherits both the advantages of the FEM-DEM and the traditional 3D-DDA method. In the 3D-NDDACP method, the contact potential (CP) originally proposed in the context of the FEM-DEM is used to deal with contact problems.

Note that the contact potential has been mentioned in many FEM-DEM literature (Munjiza and Latham 2004; Mahabadi et al. 2010; Yan et al. 2018; Lisjak et al. 2014; Zhao et al. 2018). However, due to the adoption of an explicit solution scheme, the FEM-DEM suffers from a limitation in which the time step length should be small enough to ensure the numerical stability condition (Cheng 1998). Compared with the FEM-DEM, the 3D-NDDACP method is free from the numerical stability problem, since the implicit solution scheme (Jing 1998) is used. Furthermore, contact type judgment which is not a trivial task in the traditional 3D-DDA method can be totally avoided in the 3D-NDDACP method. In addition, high accuracy for contact problems may be obtained by the 3D-NDDACP method, since the contact force in the 3D-CPDDA method is applied in the form of traction force. Finally, to overcome shortcomings of the traditional 3D-DDA method in describing the deformation of a rock block, tetrahedral FE meshes which can be effectively generated with any mature mesh generator are used to discretize each rock block. By means of the proposed 3D-NDDACP method, benchmark problems about the movement of rock block systems are fully investigated.

2 Fundamental Theory of the 3D-NDDACP Method

2.1 Displacement Function Defined for a Block

In the 3D-NDDACP method, the computational domain Ω is represented by a series of blocks with arbitrary shapes. Each block is further discretized with a series of tetrahedral elements. Regarding the i-th tetrahedral element, the displacement field $\boldsymbol{u}(\boldsymbol{x})$ for point $\boldsymbol{x}(x, y, z)$ can be described as

$$\boldsymbol{u}(\boldsymbol{x}) = \begin{pmatrix} u \\ v \\ w \end{pmatrix} = \boldsymbol{N}_i \boldsymbol{d}_i \tag{1}$$

where the shape function matrix $\boldsymbol{N}_i$ and the nodal displacement vector $\boldsymbol{d}_i$ for the i-th tetrahedral element are

$$\boldsymbol{N}_i = \begin{bmatrix} N_{i1} & 0 & 0 & N_{i2} & 0 & 0 & N_{i3} & 0 & 0 & N_{i4} & 0 & 0 \\ 0 & N_{i1} & 0 & 0 & N_{i2} & 0 & 0 & N_{i3} & 0 & 0 & N_{i4} & 0 \\ 0 & 0 & N_{i1} & 0 & 0 & N_{i2} & 0 & 0 & N_{i3} & 0 & 0 & N_{i4} \end{bmatrix} \tag{2}$$

$$N_{i1} = 1 - \xi - \eta - \zeta, N_{i2} = \xi, N_{i3} = \eta, N_{i4} = \zeta \tag{3}$$

$$\boldsymbol{d}_i^{\mathrm{T}} = \begin{bmatrix} u_{i1} & v_{i1} & w_{i1} & u_{i2} & v_{i2} & w_{i2} & u_{i3} & v_{i3} & w_{i3} & u_{i4} & v_{i4} & w_{i4} \end{bmatrix} \tag{4}$$

where N_{ij} is the shape function of j-th node, (ξ, η, ζ) are the natural coordinates of a point, and $\boldsymbol{d}_i$ represents the degree of freedoms (DOFs) of the i-th tetrahedral element.

2.2 Simultaneous Equilibrium Equations

Similar to the traditional 3D-DDA method, the simultaneous equilibrium equations in the proposed 3D-NDDACP method can also be obtained from the minimization of the total potential energy (II) of the system, and expressed as follows:

$$\boldsymbol{M}\ddot{\boldsymbol{d}} + \boldsymbol{K}\boldsymbol{d} = \boldsymbol{f}, \tag{5}$$

in which $\boldsymbol{d} = \begin{bmatrix} \boldsymbol{d}_1 & \boldsymbol{d}_2 & \cdots & \boldsymbol{d}_n \end{bmatrix}^{\mathrm{T}}$ is the global displacement vector consisting of all the tetrahedral element DOFs; $\ddot{\boldsymbol{d}}$ is the global acceleration vector equal to the second derivatives of $\boldsymbol{d}$ with regard to time t; and n is the number of all the tetrahedral elements in the system. The global matrices including mass matrix $\boldsymbol{M}$, stiffness matrix $\boldsymbol{K}$ and force vector $\boldsymbol{f}$ are calculated as

$$\begin{aligned} \boldsymbol{M} &= \int_{\Omega} \rho \boldsymbol{N}^{\mathrm{T}} \boldsymbol{N}, \boldsymbol{K} = \int_{\Omega} \boldsymbol{B}^{\mathrm{T}} \boldsymbol{D} \boldsymbol{B}, \\ \boldsymbol{f} &= \int_{\Omega} \boldsymbol{B}^{\mathrm{T}} \boldsymbol{\sigma}_0 + \int_{\Omega} \boldsymbol{N}^{\mathrm{T}} \boldsymbol{b} + \int_{\Gamma_t} \boldsymbol{N}^{\mathrm{T}} \bar{\boldsymbol{t}}, \end{aligned} \tag{6}$$

in which $\boldsymbol{b}$ is the body force per unit volume, ρ is the mass density, $\boldsymbol{D}$ is the elastic Hooke matrix, $\boldsymbol{\sigma}_0$ is the initial stress, and $\bar{\boldsymbol{t}}$ is the specified traction vector applied on Γ_t.

To solve Eq. (5), a direct time integration method, namely, the Newmark method (Zienkiewicz and Taylor 2000) is adopted. In the Newmark method, the following assumptions are made:

$$\boldsymbol{d}_{t+\Delta t} = \boldsymbol{d}_t + \Delta \boldsymbol{d}, \tag{7}$$

$$\ddot{\boldsymbol{d}}_{t+\Delta t} = \frac{\Delta \boldsymbol{d}}{\alpha \Delta t^2} - \frac{\dot{\boldsymbol{d}}_t}{\alpha \Delta t} - \left(\frac{1}{2\alpha} - 1\right)\ddot{\boldsymbol{d}}_t, \tag{8}$$

$$\dot{\boldsymbol{d}}_{t+\Delta t} = \dot{\boldsymbol{d}}_t + \Delta t(1-\delta)\ddot{\boldsymbol{d}}_t + \delta \Delta t \ddot{\boldsymbol{d}}_{t+\Delta t}, \tag{9}$$

where $\boldsymbol{d}_t$, $\dot{\boldsymbol{d}}_t$ and $\ddot{\boldsymbol{d}}_t$ represent the global displacement vector, velocity vector and acceleration vector at instant t, while $\boldsymbol{d}_{t+\Delta t}$, $\dot{\boldsymbol{d}}_{t+\Delta t}$ and $\ddot{\boldsymbol{d}}_{t+\Delta t}$ represent the global displacement vector, velocity vector and acceleration vector at instant $(t + \Delta t)$; $\Delta \boldsymbol{d}$ represents the incremental displacement vector from t to $(t + \Delta t)$; and δ and α represent the Newmark parameters, which are set to 1.0 and 0.5 in the present work to ensure an unconditional numerical stability condition.

According to Eqs. (8) and (9), $\dot{\boldsymbol{d}}_{t+\Delta t}$ can further be formulated as

$$\dot{\boldsymbol{d}}_{t+\Delta t}=\frac{\delta\Delta\boldsymbol{d}}{\alpha\Delta t}+\left(1-\frac{\delta}{\alpha}\right)\dot{\boldsymbol{d}}_t+\Delta t\left(1-\frac{\delta}{2\alpha}\right)\ddot{\boldsymbol{d}}_t \tag{10}$$

Substituting Eqs. (7), 8 and 10 into Eq. (5), the system equations at an instant $(t+\Delta t)$ can be formulated as:

$$\widetilde{\boldsymbol{K}}\Delta\boldsymbol{d}=\widetilde{\boldsymbol{f}}, \tag{11}$$

$$\widetilde{\boldsymbol{K}}=\boldsymbol{K}+\frac{\boldsymbol{M}}{\alpha\Delta t^2}, \tag{12}$$

$$\widetilde{\boldsymbol{f}}=\boldsymbol{f}_{t+\Delta t}-\boldsymbol{K}\boldsymbol{d}_t+\boldsymbol{M}\left(\frac{\boldsymbol{d}_t}{\alpha\Delta t^2}+\frac{\dot{\boldsymbol{d}}_t}{\alpha\Delta t}+\left(\frac{1}{2\alpha}-1\right)\ddot{\boldsymbol{d}}_t\right) \tag{13}$$

where $\widetilde{\boldsymbol{K}}$ and $\widetilde{\boldsymbol{f}}$ are the equivalent global stiffness matrix and force vector, respectively.

Note that the Newmark method used in the present paper satisfies the unconditional stability condition, and a large time step can be used in theory. However, due to the existence of inherent algorithm damping in the integration scheme, the accuracy of the proposed 3D-NDDACP method may be reduced. The influence of inherent algorithm damping on the accuracy of the traditional 2D-DDA method has been mentioned in (Jiang et al. 2013). According to their report, the influence of inherent algorithm damping on the accuracy of the traditional 2D-DDA method can be effectively reduced by using small time step. We will investigate the effect of time step length on the accuracy of the numerical solution of the 3D-NDDACP method in Sect. 4.2.1.

3 Contact Force Formulation

3.1 Normal Contact Force

In the proposed 3D-NDDACP method, rock blocks, which can be in any shape, are discretized into a series of tetrahedral elements. Hence, the contact force between any two rock blocks can be obtained by sum all the contact forces caused by the contact between the tetrahedral elements belonging to the two rock blocks.

The normal contact forces between two tetrahedral elements are calculated by a potential function method proposed by (Munjiza and Andrews 2000). The distributed normal contact force ($\mathrm{d}\boldsymbol{f}_n$) is computed according to the overlap volume ($\mathrm{d}V$) between the contactor element (β_c) and the target element (β_t):

$$\mathrm{d}\boldsymbol{f}_n=k_n\left[\mathrm{grad}\varphi_c\left(\boldsymbol{P}_c\right)-\mathrm{grad}\varphi_t\left(\boldsymbol{P}_t\right)\right]\mathrm{d}V \tag{14}$$

where k_n is the normal penalty parameter; $\boldsymbol{P}_c$ and $\boldsymbol{P}_t$ are the overlapping points of β_c and β_t; and φ is the corresponding contact potential function.

By integrating the distributed normal contact force $\mathrm{d}\boldsymbol{f}_n$ over the overlapping volume of β_c and β_t, the total normal contact force $\boldsymbol{f}_n$ between β_c and β_t can be computed

$$\boldsymbol{f}_n=\iiint_{\beta_c\cap\beta_t}k_n\left[\mathrm{grad}\varphi_c\left(\boldsymbol{P}_c\right)-\mathrm{grad}\varphi_t\left(\boldsymbol{P}_t\right)\right]\mathrm{d}V \tag{15}$$

As proven by (Munjiza and Andrews 2000), the normal contact force $\boldsymbol{f}_n$ in Eq. (15) can also be written as an integral over the surface boundaries $S_{\beta_c\cap\beta_t}$ of the overlapping volume $\beta_c\cap\beta_t$, leading to

$$\boldsymbol{f}_n=k_n\iint_{S_{\beta_c\cap\beta_t}}\boldsymbol{n}_S\left[\varphi_c\left(\boldsymbol{P}_c\right)-\varphi_t\left(\boldsymbol{P}_t\right)\right]\mathrm{d}S \tag{16}$$

where $\boldsymbol{n}_S$ is unit outward normal vector to the outer boundary surface $S_{\beta_c\cap\beta_t}$ of the overlapping volume $\beta_c\cap\beta_t$.

3.2 Shear Contact Force

According to the Mohr–Coulomb criterion, shear contact force between two tetrahedral elements can be expressed as

$$\boldsymbol{f}'^{t+\Delta t}_{\tau}=\boldsymbol{f}^t_{\tau}-k_s\Delta u_{\tau}S_B \tag{17}$$

where $\boldsymbol{f}'^{t+\Delta t}_{\tau}$ represents the trial value of shear contact force at time instant $(t+\Delta t)$; $\boldsymbol{f}^t_{\tau}$ is the shear contact force at time instant t; k_s is the shear penalty parameter; S_B is the contact area; and Δu_{τ} is the tangential relative displacement increment within Δt.

If the trial shear contact force satisfies $\left|\boldsymbol{f}'^{t+\Delta t}_{\tau}\right|\le\mu\left|\boldsymbol{f}_n\right|$, then

$$\boldsymbol{f}^{t+\Delta t}_{\tau}=\boldsymbol{f}'^{t+\Delta t}_{\tau} \tag{18}$$

Otherwise, it is calculated as follows

$$\boldsymbol{f}^{t+\Delta t}_{\tau}=\frac{\boldsymbol{f}'^{t+\Delta t}_{\tau}}{\left|\boldsymbol{f}'^{t+\Delta t}_{\tau}\right|}\mu\left|\boldsymbol{f}_n\right| \tag{19}$$

Here, μ represents the frictional coefficient.

According to the principle of minimum potential energy, the equivalent load vectors from the normal contact force and shear contact force can be obtained, see details in (Xu et al. 2020).

The values of the normal penalty parameter k_n in Eq. (15) and the shear penalty parameter k_s in Eq. (17) may have influence on the performance of the proposed 3D-NDDACP method for contact problems. Hence, the optimal values for k_n and k_s should be determined. The corresponding content will be discussed in Sect. 4.2.

Note that in each step the contact treatment between blocks is handled by contact forces rather than a contact matrix, which are calculated according to the updated state

of the rock block system of the previous step. This treatment may bring some explicit features over time step. Similar practices can also be found by (Zhao et al. 2017).

4 Numerical Examples

In the traditional 3D-DDA method, the first-order displacement function is used to model the deformation of a rock block. Hence, the strain and stress of each rock block are constants and are equally distributed. In the proposed 3D-NDDACP method, tetrahedral finite element meshes are used to discretize each rock block. The strain and stress of each rock block computed by the 3D-NDDACP method are no more constants. Hence, the proposed 3D-NDDACP method can better capture the deformation of rock blocks than the traditional 3D-NDDACP method. In the following content, we mainly focus on the testing of the proposal method for 3D rock block contact problems.

4.1 Momentum Conservation Test

As the first example, a rock block collision test shown in Fig. 1 is considered. The sizes of Block A and Block B are both 1 m × 1 m × 1 m. The distance between Block A and Block B is 0.02 m. At time instant 0 s, Block A with an initial horizontal speed (1 m/s) starts sliding along the frictionless plate towards the stationary Block B. Shown in Fig. 2 is the discretized model for this momentum conservation test.

In the computation, two cases, namely, Case 1 and Case 2 are considered. In Case 1, the mechanical parameters for Block A, Block B and the plate are set as the same values, namely, Young's modulus $E = 20$ GPa, Poisson's ratio$\nu = 0.25$ and density $\rho = 2650$ kg/m^3; In Case 2, the density for Block B is set as 1325 kg/m^3, and the rest parameters are set as the same values in Case 1. All the outer surfaces (except the up surface) of the plate are constrained in the normal direction with very stiff springs with a stiffness of 10^6E. Note that in the proposed 3D-NDDACP method, the

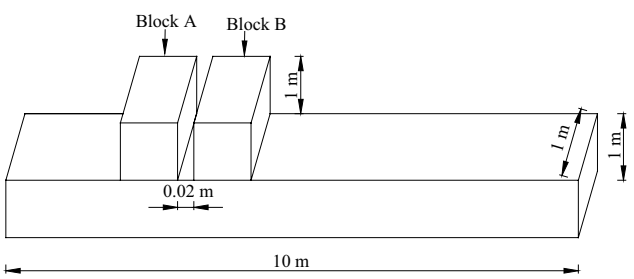

Fig. 1 A rigid block collision example: Block A having initial velocity V_0 slides toward Block B

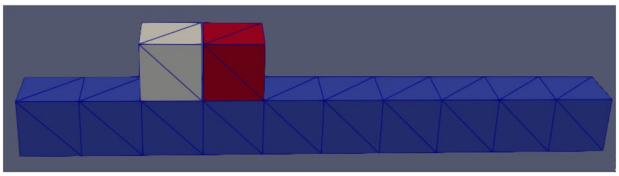

Fig. 2 Discretized model used for the momentum conservation test

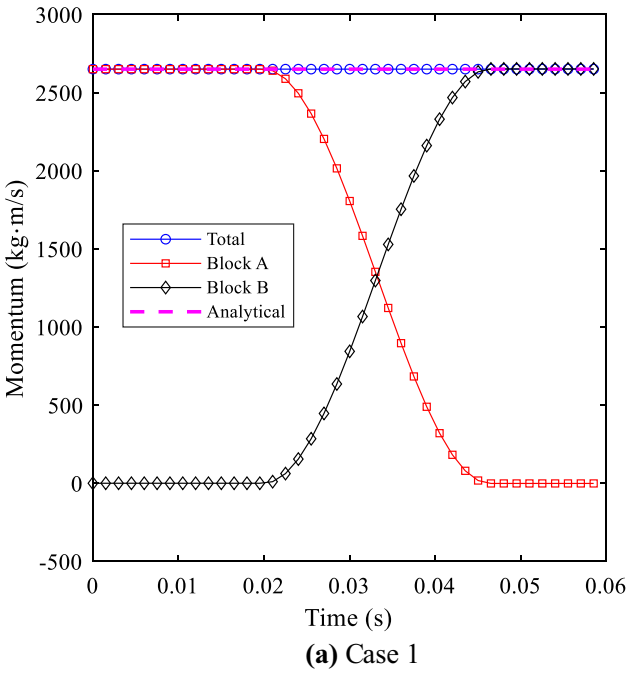

(a) Case 1

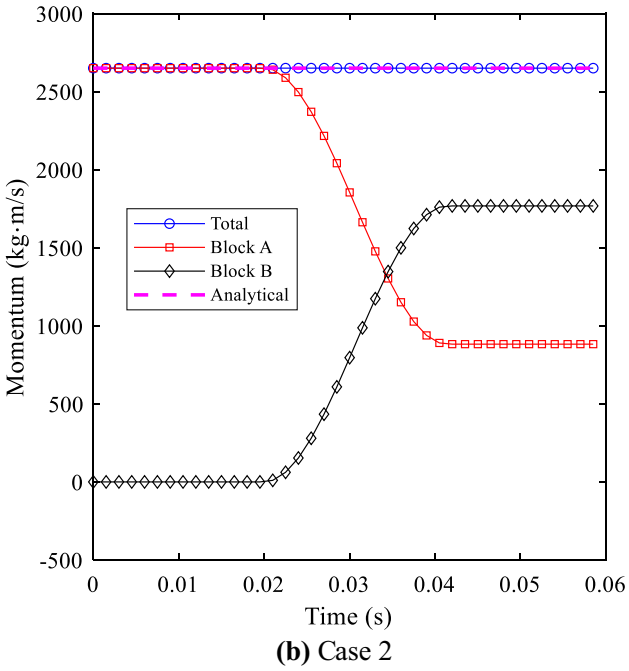

(b) Case 2

Fig. 3 Computed momentum versus time step

penalty method used in the traditional DDA method is also adopted to impose displacement boundary conditions. The time step length Δt is taken as a constant, namely, 1.0×10^{-6} s.

In theory, Block A will collide Block B at time instant 0.02 s. In addition, the block system should satisfy the law of momentum conservation and kinetic energy conservation. To be more specific: (1) The global horizontal momentum should always be 2650 kg m/s even after block A colliding with block B; (2) In Case 1, the velocities for Block A and Block B should be 1 m/s and 0 m/s before collision, and be 0 m/s and 1 m/s after collision; and (3) In Case 2, the velocities for Block A and Block B should be 1 m/s and 0 m/s before collision, and be 1/3 (0.3333) m/s and 4/3 (1.3333) m/s after the collision.

The calculated total horizontal momentum, horizontal momentums of Block A and B and analytical value of total horizontal momentum versus time are plotted in Fig. 3. It is shown that the calculated total horizontal momentums are identical to the analytical values, which means that the proposed 3D-NDDACP method passes this momentum conversation test.

Furthermore, the values of horizontal momentum and velocity for Blocks A and B are also listed in Tables 1 and 2. It is shown that the values of momentum and velocity for Blocks A and B computed with the proposed method are all very close to the analytical values.

4.2 Sliding Problem

For the second example, a small tri-prism block staying on a ramp is considered, as shown in Fig. 4. The slope angle of the ramp is α. In the computation, the tri-prism block and the ramp's material parameters are: Young's

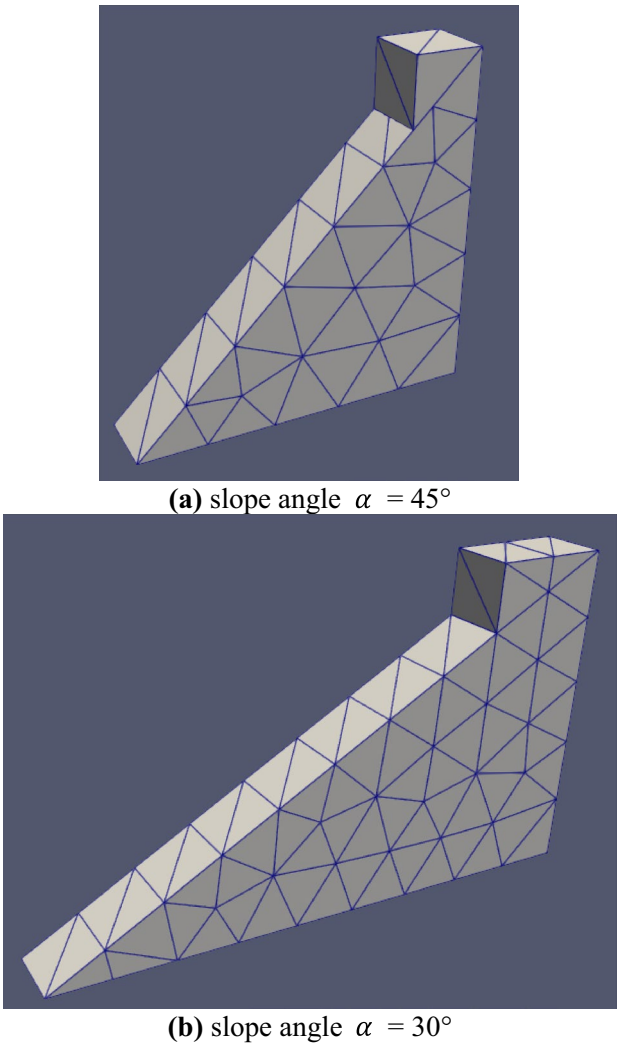

(a) slope angle $\alpha = 45°$

(b) slope angle $\alpha = 30°$

Fig. 4 A block slides along a ramp

Table 1 Computed horizontal momentums of the two blocks (unit: kg m/s)

Case number	Methods	Before collision			After collision		
		Block A	Block B	Total	Block A	Block B	Total
Case 1	3D-NDDACP	2650.0000	0.0000	2650.0000	− 1.3250	2651.3250	2650.0000
	Theoretical value	2650.0000	0.0000	2650.0000	0.0000	2650.0000	2650.0000
Case 2	3D-NDDACP	2650.0000	0.0000	2650.0000	882.3808	1767.6210	2650.0018
	Theoretical value	2650.0000	0.0000	2650.0000	883.3333	1766.6667	2650.0000

Table 2 Computed horizontal velocities of the two blocks (unit: m/s)

Case number	Methods	Before collision		After collision	
		Block A	Block B	Block A	Block B
Case 1	3D-NDDACP	1.0000	0.0000	− 0.0005	1.0005
	Theoretical value	1.0000	0.0000	0.0000	1.0000
Case 2	3D-NDDACP	1.00000	0.00000	0.3330	1.3341
	Theoretical value	1.00000	0.00000	0.3333	1.3333

modulus $E = 200$ GPa, Poisson's ratio $\nu = 0.25$ and density $\rho = 2650$ kg/m^3. The bottom surface of the ramp is fixed, while the other surfaces except the surface contacting the tri-prism block are all constrained in the normal direction. Due to the self-weight effect, the tri-prism block may slide along the ramp. To record the displacement time history of the tri-prism block, a monitoring point located at its center is used.

The analytical sliding displacement of the tri-prism block (S) at time instant t (s) can be expressed as:

$$S = 0.5(\sin\alpha - \mu\cos\alpha)gt^2 \tag{20}$$

where g represents the gravity speed (9.8 m/s^2); μ represents the frictional coefficient which can be expressed as $\tan(\phi/180°)$. Here, ϕ represents the friction angle between the tri-prism block and ramp.

4.2.1 Influence of Normal Penalty Parameter on acCuracy of Numerical Solution

To analyze the influence of normal penalty parameter value on the accuracy of the proposed 3D-NDDACP method, six different values of normal penalty parameter (k_n) are considered, namely, k_n will be separately set to $1.0 \times 10^{-1}E$, $1.0 \times 10^{-2}E$, ⋯, and $1.0 \times 10^{-6}E$. In this section, only the case for slope angle $\alpha = 45°$ and friction angle $\phi = 0°$ is considered.

Figure 5a shows the relative displacement errors under different values of the normal penalty parameter (k_n) for time step length $\Delta t = 1.0 \times 10^{-4}$ s. For a clearer comparison, Fig. 5a is decomposed into Fig. 5b–f. As can be seen in Fig. 5b–e, the relative errors of displacement time history gradually decrease as the value of k_n decreases. When the value of k_n is set as $1.0 \times 10^{-5}E$, the magnitude of relative errors of displacement time history is only 10^{-4}. However, when the value of k_n is set as $1.0 \times 10^{-6}E$, the biggest magnitude of relative errors of displacement time history reaches 10^{-3} (Fig. 5f). Hence, the optimal value for k_n in this case is $1.0 \times 10^{-5}E$.

Furthermore, to analyze the effect of time step length on the accuracy of the numerical solution, a smaller time step length, namely, $\Delta t = 1.0 \times 10^{-5}$ s, is also considered. Figure 6a shows the relative displacement errors under different values of the normal penalty parameter (k_n) for time step length $\Delta t = 1.0 \times 10^{-5}$ s. Figure 6a is also decomposed into five subfigures, namely, Fig. 6b–f for a clearer comparison. As can be seen in Fig. 6b–e, the magnitudes of relative errors of displacement time history are all only 10^{-4} for $k_n = 1.0 \times 10^{-1}E$, $1.0 \times 10^{-2}E$, ⋯, and $1.0 \times 10^{-5}E$. Even for $k_n = 1.0 \times 10^{-6}E$, the magnitude of relative errors of displacement time history are also only 10^{-4} except for time instant t is close to 0.024 s. Similar to the case with $\Delta t = 1.0 \times 10^{-4}$ s, the optimal value for k_n is also $1.0 \times 10^{-5}E$ for the case with $\Delta t = 1.0 \times 10^{-5}$ s.

To better illustrate the influence of time step length Δt on the accuracy of the numerical solution for $k_n = 1.0 \times 10^{-5}E$, Fig. 7 is plotted. As can be seen in Fig. 7, the magnitude of relative errors of displacement time history are all only 10^{-4} for $\Delta t = 1.0 \times 10^{-4}$ s and 1.0×10^{-5} s. The accuracy of the numerical solution for $\Delta t = 1.0 \times 10^{-5}$ s is generally better than that for $\Delta t = 1.0 \times 10^{-4}$ s. The time step length has some influence on the accuracy of the numerical solution.

Base on the above discussion, the value of the normal penalty parameter (k_n) will be set to $1.0 \times 10^{-5}E$ in the following content.

4.2.2 Influence of Shear Penalty Parameter on Accuracy of Numerical Solution

To analyze the influence of the shear penalty parameter value on the accuracy of the proposed 3D-NDDACP method, four different values of the shear penalty parameter k_s are considered, namely, k_s will be separately set to $1.0 \times 10^{-0}E$, $1.0 \times 10^{-1}E$, $1.0 \times 10^{-2}E$, and $1.0 \times 10^{-3}E$.

In this section, two cases, namely, Case I and Case II are considered. For Case I, slope angle $\alpha = 45°$ and friction angle $\phi = 35°$; and for Case II, slope angle $\alpha = 30°$ and friction angle $\phi = 25°$. For both Case I and Case II, the time step length Δt are all set to 1.0×10^{-5} s.

Figure 8a shows the relative displacement errors under different values of the shear penalty parameter (k_s) for Case I. For a clearer comparison, Fig. 8a is decomposed into Fig. 8b–d. As can be seen in Fig. 8b–d, the curves of relative errors for $k_s = 1.0 \times 10^{-2}E$, $1.0 \times 10^{-1}E$ and $1.0 \times 10^{-0}E$ are basically coincide to each other. The magnitude of relative errors of displacement time history is only 10^{-3}. However, the maximum value of relative errors of displacement time history for $k_s = 1.0 \times 10^{-3}E$ is close to 0.14.

Figure 9a shows the relative displacement errors under different values of the shear penalty parameter (k_s) for Case II. For a clearer comparison, Fig. 9a is decomposed into Fig. 9b–d. As can be seen in Fig. 9b–d, the curves of relative errors for $k_s = 1.0 \times 10^{-2}E$, $1.0 \times 10^{-1}E$ and $1.0 \times 10^{-0}E$ are also basically coincide to each other. The magnitude of relative errors of displacement time history is only 10^{-2}. Note that the maximum value of relative errors of displacement time history for $k_s = 1.0 \times 10^{-3}E$ is close to 0.4.

Base on the above discussion, the shear penalty parameter k_s can be set to $1.0 \times 10^{-2}E$, $1.0 \times 10^{-1}E$ and $1.0 \times 10^{-0}E$. In the following section, the normal penalty parameter k_n will be set to $1.0 \times 10^{-5}E$, while the shear penalty parameter k_s will be set to $1.0 \times 10^{-1}E$.

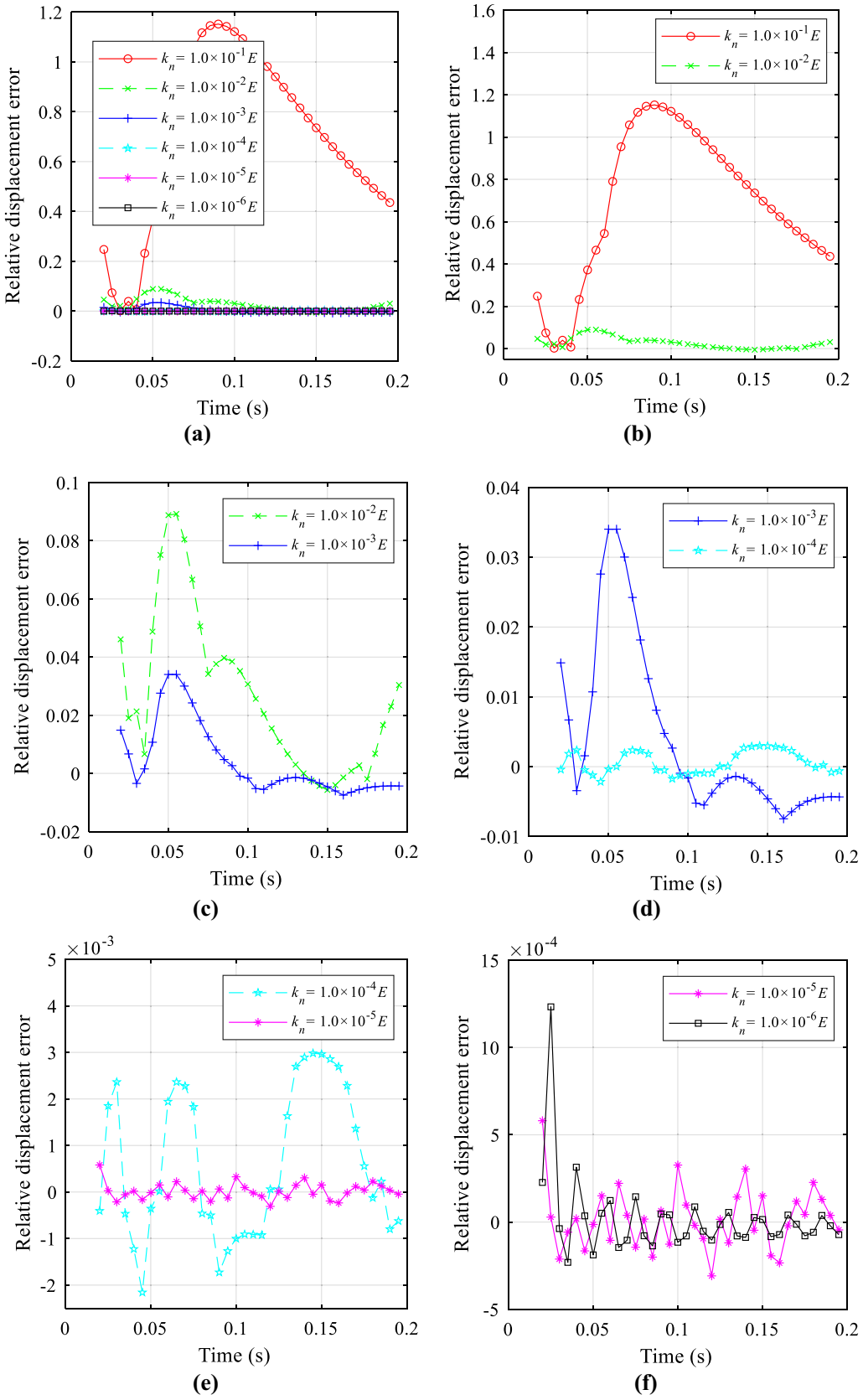

Fig. 5 Relative displacement errors under different values of normal penalty parameter (k_n) for time step length $\Delta t = 1.0\times10^{-4}$ s and slope angle $\alpha = 45°$

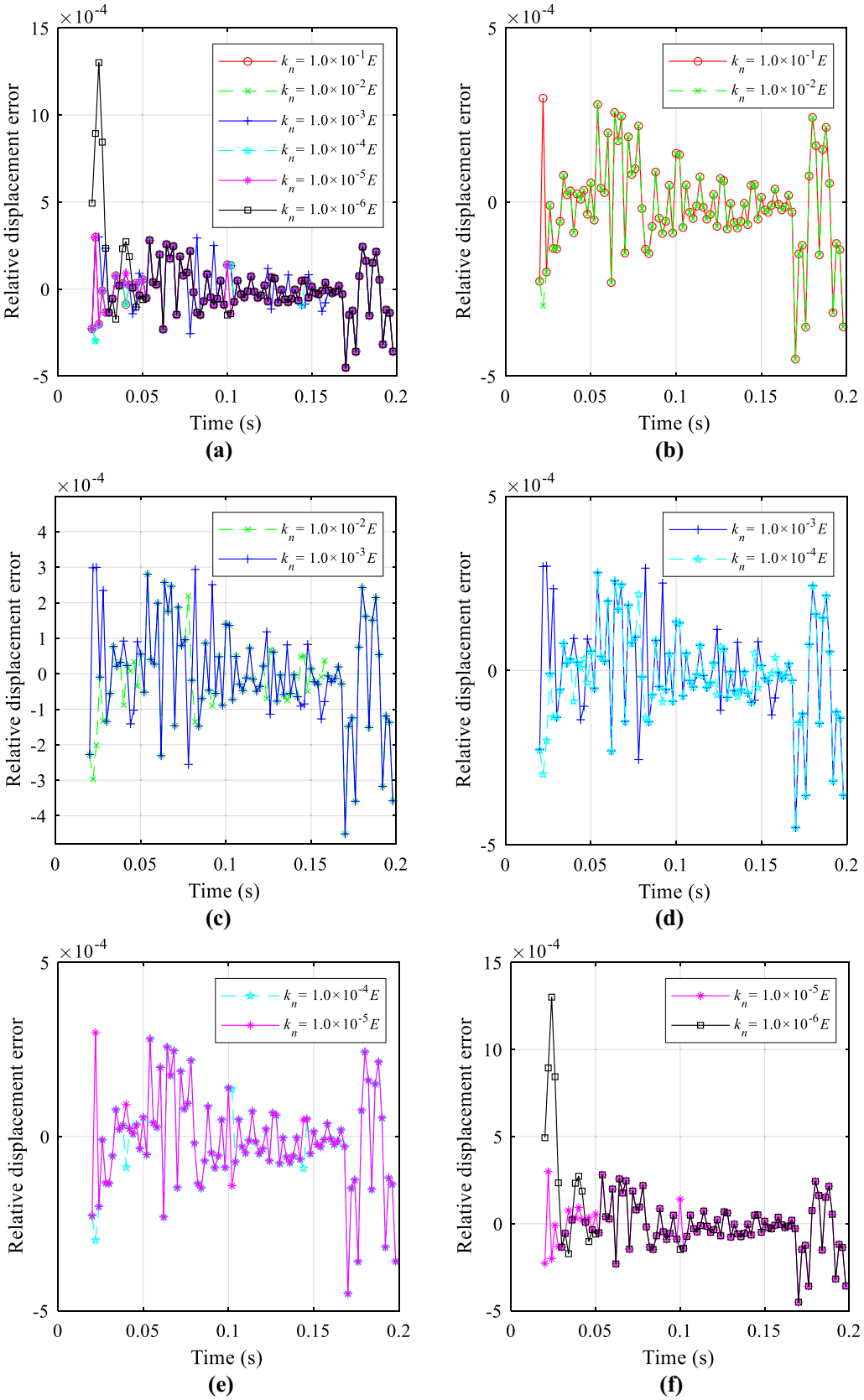

Fig. 6 Relative displacement errors under different values of normal penalty parameter (k_n) for time step length $\Delta t = 1.0 \times 10^{-5}$ s and slope angle $\alpha = 45°$

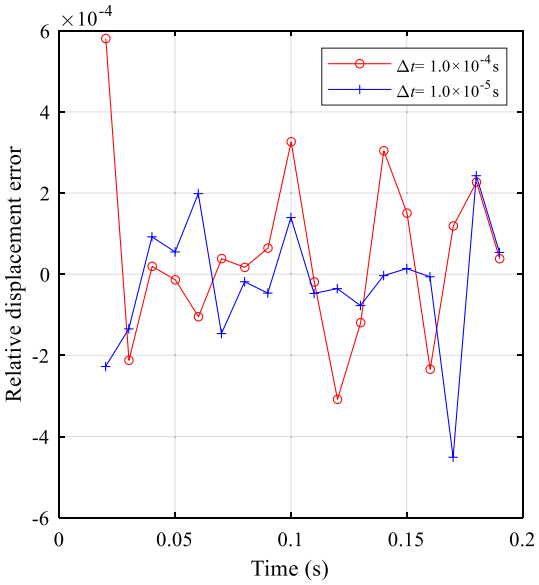

Fig. 7 Relative displacement errors under different time step length Δt for slope angle $\alpha = 45°$ and friction angle $\phi = 0°$

4.2.3 Influence of Friction Coefficient on Accuracy of the Numerical Solution

In this section, the influence of friction coefficient value on the accuracy of the proposed 3D-NDDACP method is analyzed. In the computation, the time step length Δt, normal penalty parameter k_n and shear penalty parameter k_s are set to 1.0×10^{-5} s, $1.0 \times 10^{-5}E$ and $1.0 \times 10^{-1}E$, respectively.

Two cases, namely, Case III and Case IV are considered. For Case III, slope angle $\alpha = 45°$ and friction angle $\phi = 0° \sim 35°$; and for Case IV, slope angle $\alpha = 30°$ and friction angle $\phi = 0° \sim 25°$. For both Case III and Case IV, the time step length Δt are all set to 1.0×10^{-5} s.

Figure 10 shows the relative displacement errors under different friction angles (ϕ) corresponding to Case III. As can be seen in Fig. 10, the oscillation of the relative error curve happens for all eight friction angles. Additionally, for each friction angle, the magnitude of relative error gradually decreases to very small values as time goes on. Similar conclusions also hold for Case IV, as shown in Fig. 11.

Fig. 8 Relative displacement errors under different values of shear penalty parameter (k_s) for time step length $\Delta t = 1.0 \times 10^{-5}$ s, slope angle $\alpha = 45°$and friction angle ϕ=35°

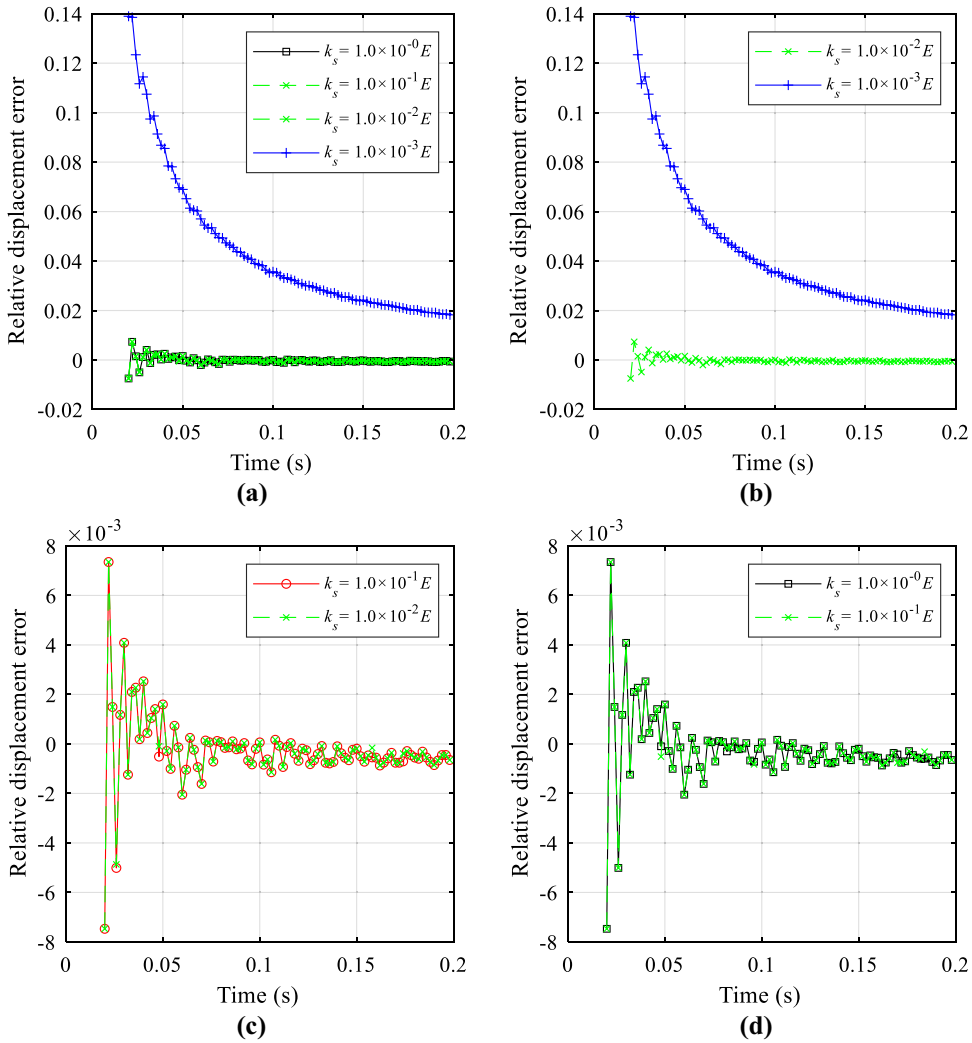

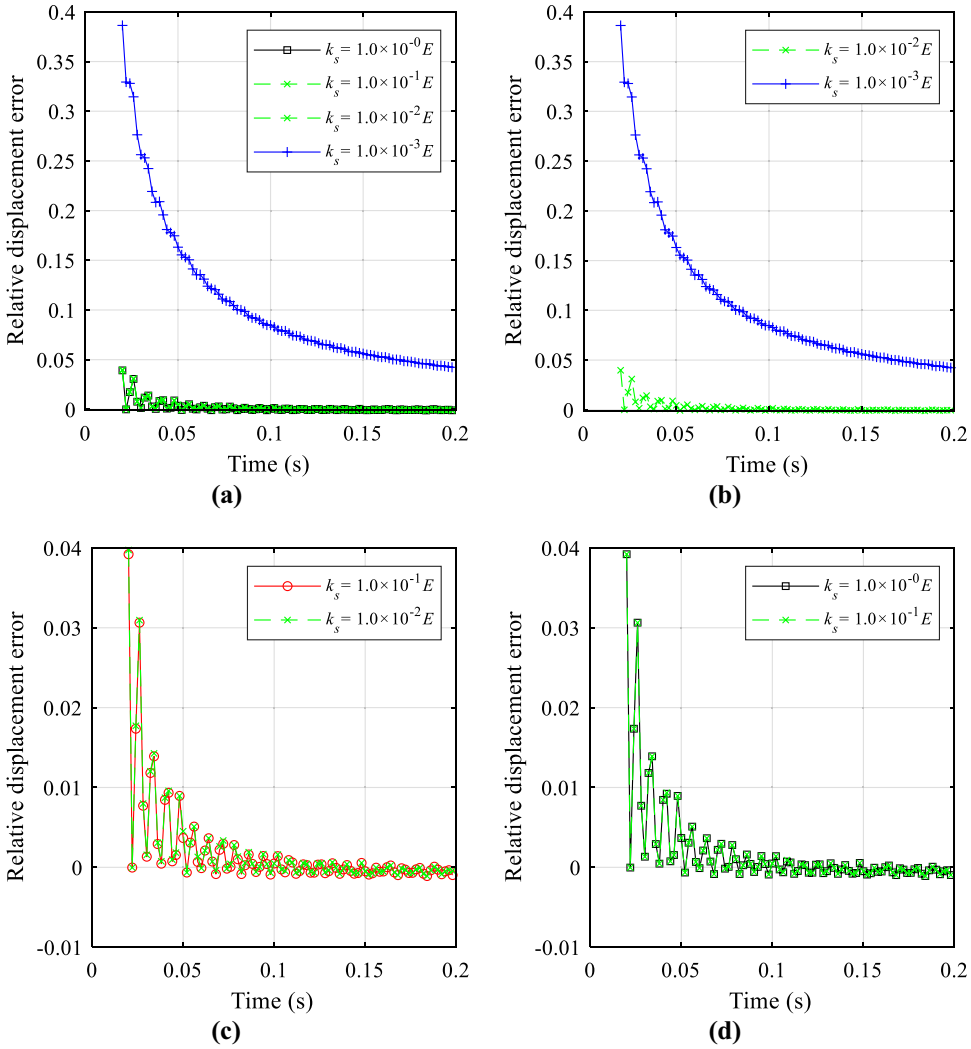

Fig. 9 Relative displacement errors under different values of shear penalty parameter (k_s) for time step length $\Delta t = 1.0 \times 10^{-5}$ s, slope angle $\alpha = 30°$ and friction angle $\phi = 25°$

4.3 A Complex Block System

As the last example, we consider a complex polyhedral block system, as shown in Fig. 12. The computational model consists of a cubic base and a series of polyhedral rock blocks. The polyhedral rock blocks are generated by cutting a column with the size of 5 m × 5 m × 10 m using a joint set. The material parameters of the blocks and the cubic base are: Young's modulus $E = 200$ GPa, Poisson's ratio $\nu = 0.25$, density $\rho = 2650$ kg/m^3. The time step length Δt is set to 1.0×10^{-4} s. In the computation, the four side surfaces and the bottom surface of the cubic base are constrained in the normal direction.

Three scenarios corresponding to different friction angles ($\phi = 0°$, 5° and 10°) are investigated. The kinetic movements of the block system on the cubic base under gravity load are recorded. The gravity load is treated as an external force which is added suddenly at the beginning of the calculation. The block geometries at different time instants for the first scenario ($\phi = 0°$), the second scenario ($\phi = 5°$) and the third scenario ($\phi = 10°$) are separately plotted in Figs. 13, 14 and 15.

Due to the frictionless condition in the first scenario, the rock blocks move freely under the gravity load. Note that this scenario has also been investigated by (Zheng et al. 2020). The block geometries at different instants predicted with the present numerical model agree well with those presented by (Zheng et al. 2020).

For the second scenario and the third scenario, the rock blocks cannot move freely under the gravity load, due to the influence of friction between blocks. At 0.7 s, the maximum values of x-displacement for the second scenario and the third

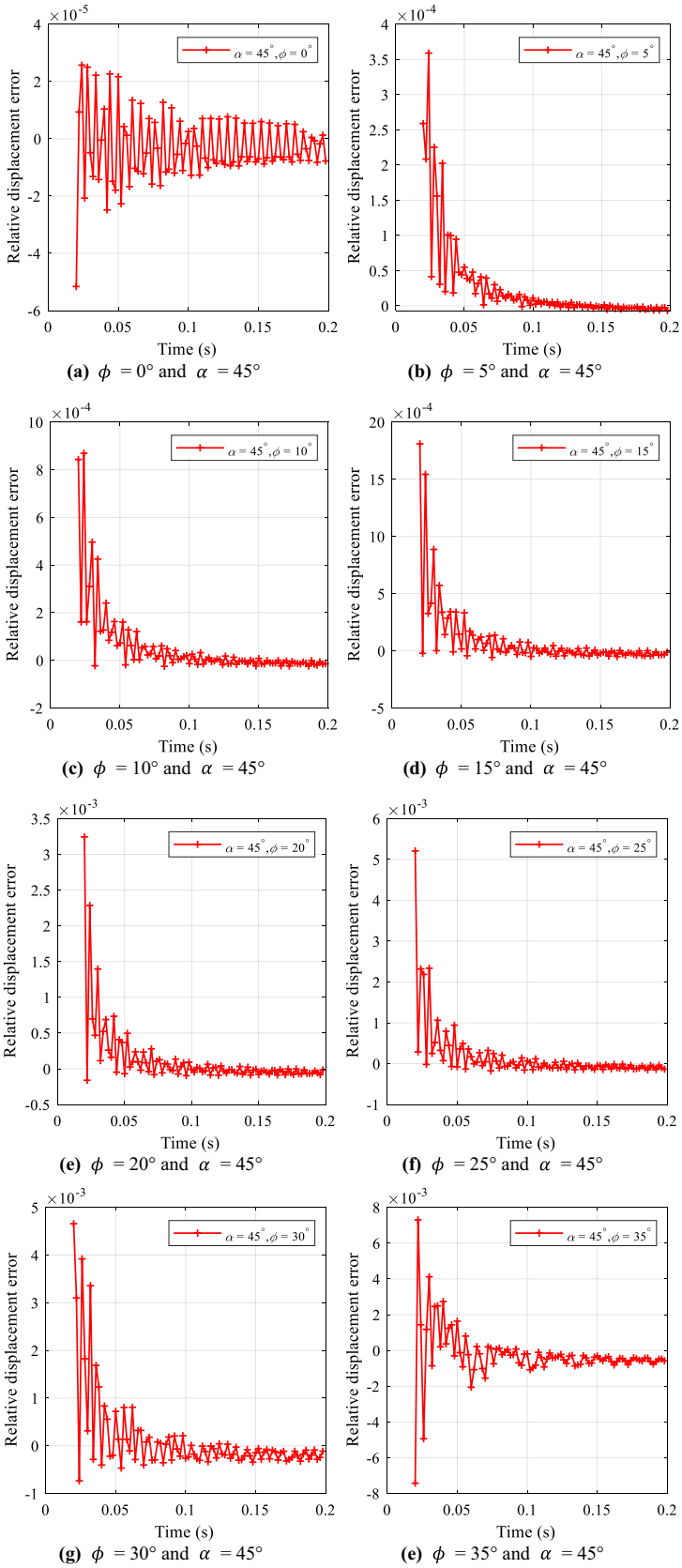

Fig. 10 Relative displacement errors under different friction angles (ϕ) for time step length $\Delta t = 1.0 \times 10^{-5}$ s and slope angle $\alpha = 45°$

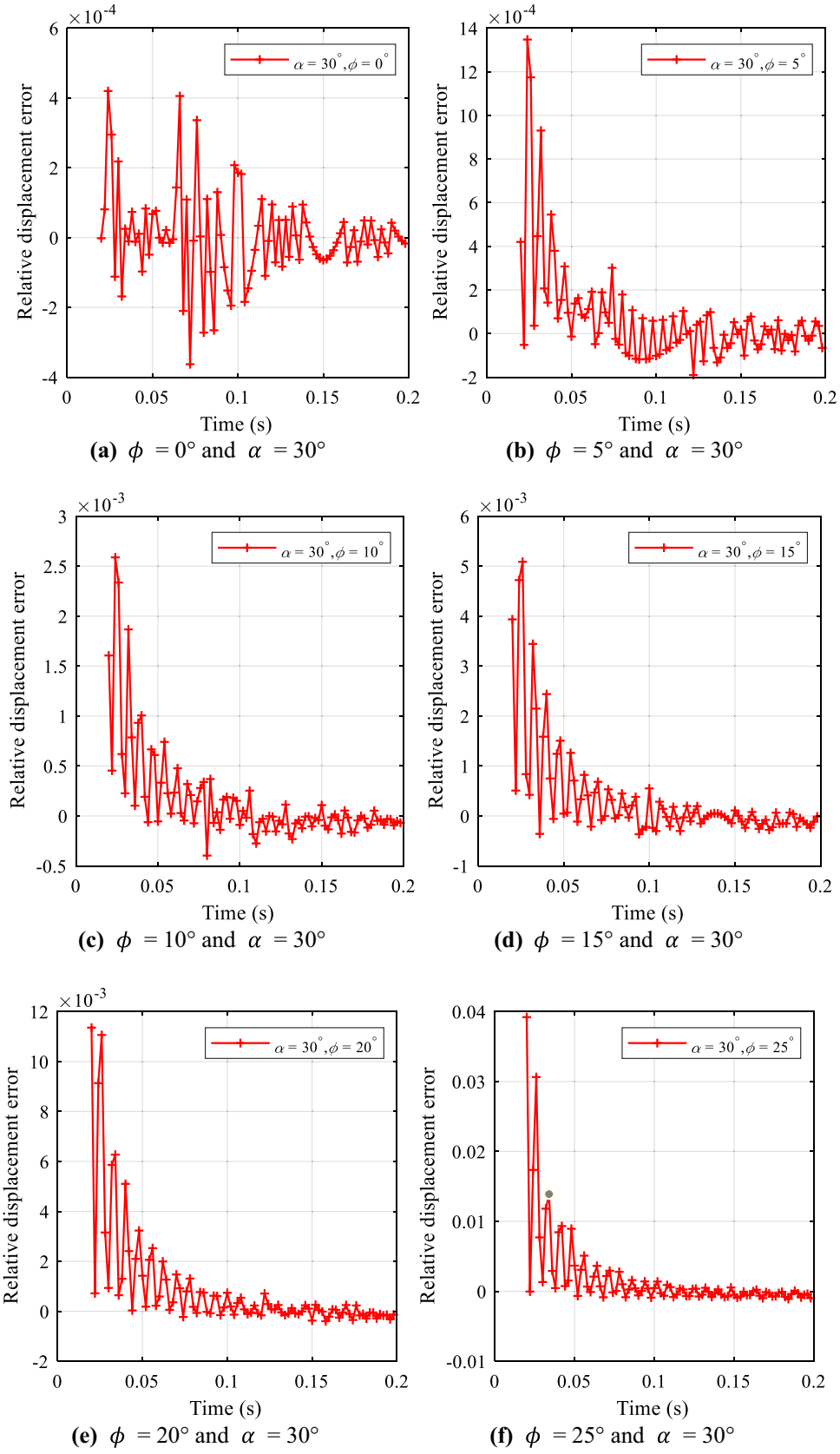

(a) $\phi = 0°$ and $\alpha = 30°$ **(b)** $\phi = 5°$ and $\alpha = 30°$

(c) $\phi = 10°$ and $\alpha = 30°$ **(d)** $\phi = 15°$ and $\alpha = 30°$

(e) $\phi = 20°$ and $\alpha = 30°$ **(f)** $\phi = 25°$ and $\alpha = 30°$

Fig.11 Relative displacement errors under different friction angles (ϕ) for time step length $\Delta t = 1.0 \times 10^{-5}$ s and slope angle $\alpha = 30°$

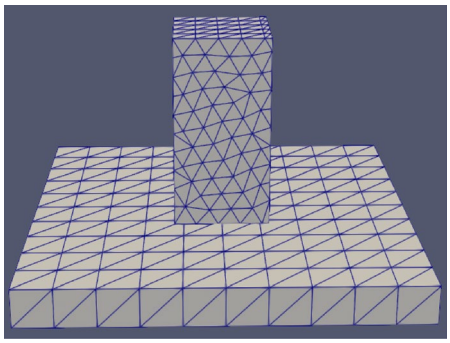

(a) Discretized model

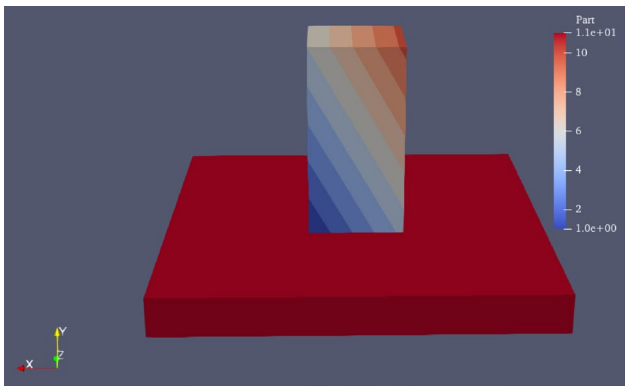

(b) the initial block geometry (block number plot)

Fig. 12 A polyhedral block system

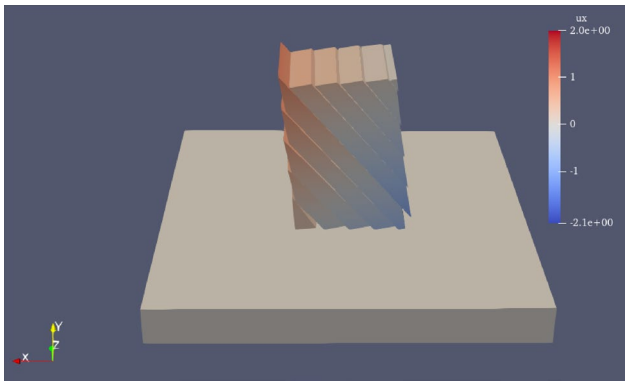

(a) the block geometry at 0.5 s (*x*-displacement plot)

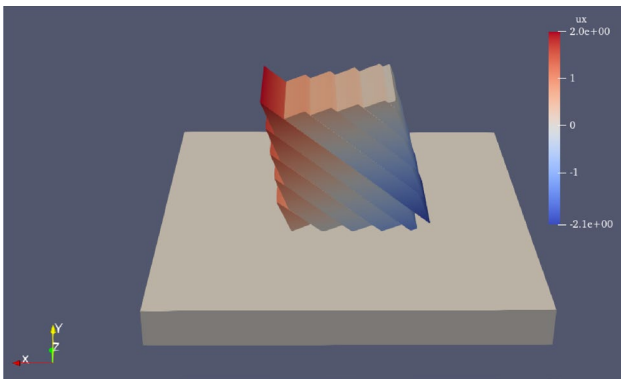

(b) the block geometry at 0.7 s (*x*-displacement plot).

Fig. 13 The block geometry at different instants for the first scenario ($\phi = 0°$)

scenario are 1.970 m and 1.886 m respectively, which are smaller than that for the first scenario (1.983 m).

5 Conclusions

To better analyze rock mechanics problems, a nodal-based 3D discontinuous deformation analysis method with the contact potential (3D-NDDACP) is developed. In the proposed numerical model, tetrahedral FE meshes which can be effectively generated are adopted to discretize each rock block. Additionally, the contact potential is used to compute contact forces between any two rock blocks. The proposed numerical model has the following advantages:

A) Due to the adoption of tetrahedral FE meshes in each rock block, the continuum mechanics principles used in FEM may be used in the proposed 3D-NDDACP method. By refining the FE mesh in each rock block, the deformation ability can be enhanced, while the stress distribution can be refined.
B) According to the definition of contact potential, there is no need to distinguish contact types between any two blocks. Hence, the contact force can be directly computed in the proposed 3D-NDDACP method. However, in the traditional 3D-DDA method, the contact type should be determined before computing the contact force. Note that the determination of contact types in the traditional 3D-DDA method is not a tractable task, since many different contact types including the point-to-point contact, point-to-edge contact, point-to-face contact or edge-to-edge contact are involved.
C) In the traditional 3D-DDA method, the contact force is first treated as concentrated force, and then added to the global force vector. However, in the proposed 3D-NDDACP method, the contact force is in direct proportion to the contact volume, and is treated as a traction force before adding into the global force vector. The numerical examples investigated in the present work indicate that the proposed 3D-NDDACP method can accurately simulate contact problems.
D) The open-close iteration processes are not needed in the proposed 3D-NDDACP method. Hence, the implementation of the 3D-NDDACP method is much easier than that of the traditional 3D-DDA method.

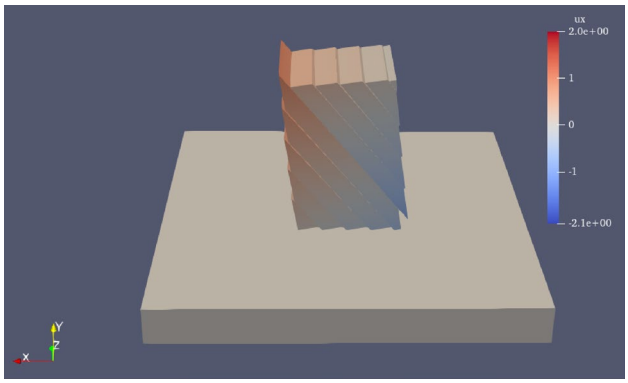

(a) the block geometry at 0.5 s (*x*-displacement plot)

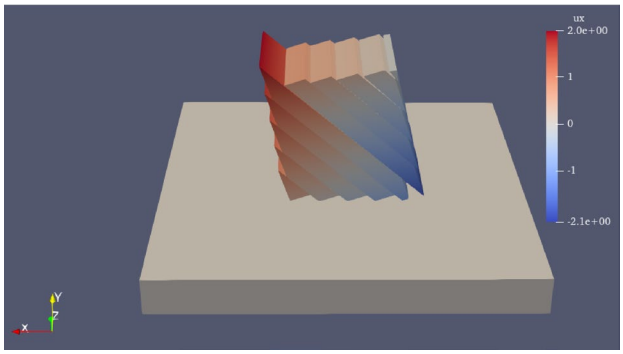

(b) the block geometry at 0.7 s (*x*-displacement plot).

Fig. 14 The block geometry at different instants for the second scenario ($\phi = 5°$)

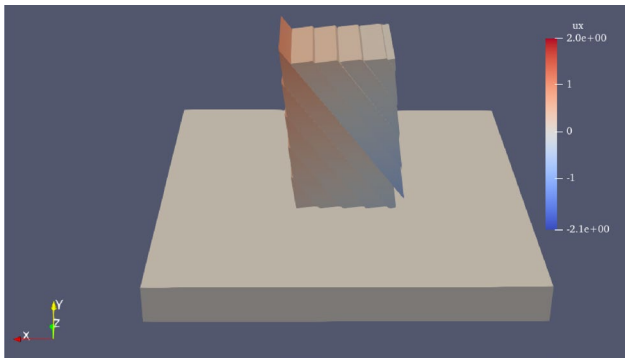

(a) the block geometry at 0.5 s (*x*-displacement plot)

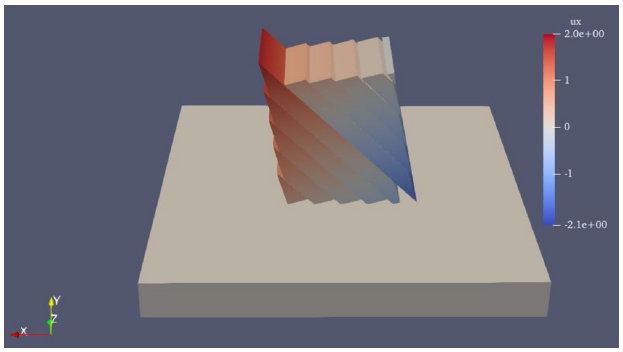

(b) the block geometry at 0.7 s (*x*-displacement plot).

Fig. 15 The block geometry at different instants for the third scenario ($\phi = 10°$)

E) In each time step the contact treatment between blocks is handled by contact forces. Compared with the traditional DDA method, this treatment in the proposed 3D-NDDACP method will bring some explicit features over the time step, which means that a small time step length may needed to ensure accuracy requirement. However, according to our test (Sect. 4.2.1), even when the time step length Δt is set to 1.0×10^{-4}, the magnitude of relative errors of displacement time history is only 10^{-4}, which means that the influence of explicit features from the contact force is limited.

Apart from the abovementioned advantages, the proposed 3D-NDDACP method is very suitable for solving rock fracturing problems. In our future work, the current version of the 3D-NDDACP method will be further improved for the rock fracturing modelling.

Acknowledgements This study is supported by the Youth Innovation Promotion Association CAS, China, under grant no. 2020327; the Young Top-notch Talent Cultivation Program of Hubei Province; and the National Natural Science Foundation of China, under the grant numbers 12072357, 12272393 and 12202024.

Data Availability The data are available from the corresponding author on reasonable request.

References

Bao HR, Hatzor YH, Huang X (2012) A new viscous boundary condition in the two-dimensional discontinuous deformation analysis method for wave propagation problems. Rock Mech Rock Eng 45:919–928

Beyabanaki SAR, Mikola RG, Hatami K (2008) Three-dimensional discontinuous deformation analysis (3-D DDA) using a new contact resolution algorithm. Comput Geotech 35(3):346–356

Beyabanaki SAR, Jafari A, Biabanaki SOR, Yeung MR (2009) Nodal-based three-dimensional discontinuous deformation analysis (3-D DDA). Comput Geotech 36:359–372

Cheng YM (1998) Advancements and improvement in discontinuous deformation analysis. Comput Geotech 22(2):153–163

Choo LQ, Zhao Z, Chen H, Tian Q (2016) Hydraulic fracturing modeling using the discontinuous deformation analysis (DDA) method. Comput Geotech 76:12–22

Feng XX, Jiang QH, Zhang HC, Zhang XB (2021) Study on the dynamic response of dip bedded rock slope using discontinuous deformation analysis (DDA) and shaking table tests. Int J Numer Anal Methods Geomech 45(3):411–427

Goodman RE (1976) Methods of geological engineering in discontinuous rocks. Wiley, New York

Gu J, Zhao ZY (2009) Considerations of the discontinuous deformation analysis on wave propagation problems. Int J Numer Anal Meth Geomech 33(12):1449–1465

Jiang QH, Yeung MR (2004) A model of point-to-face contact for three-dimensional discontinuous deformation analysis. Rock Mech Rock Eng 37(2):95–116

Jiang QH, Chen YF, Zhou CB, Yeung MR (2013) Kinetic energy dissipation and convergence criterion of discontinuous deformations analysis (DDA) for geotechnical engineering. Rock Mech Rock Eng 46(6):1443–1460

Jiao YY, Zhang XL, Zhao J, Liu QS (2007) Viscous boundary of DDA for modeling stress wave propagation in jointed rock. Int J Rock Mech Min Sci 44(7):1070–1076

Jing L (1998) Formulation of discontinuous deformation analysis (DDA)-an implicit discrete element model for block systems. Eng Geol 49(3–4):371–381

Jing L (2003) A review of techniques, advances and outstanding issues in numerical modelling for rock mechanics and rock engineering. Int J Rock Mech Min Sci 40(3):283–353

Kottenstette JT (1999) DDA analysis of the RCC modification for Pueblo Dam. In Proc., ICADD-3: Third Int. Conf. on Analysis of Discontinuous Deformation-From Theory to Practice, edited by B. Amadei. American Rock Mechanics Association, Balkema, Washington DC. pp. 127–132

Lin CT, Amadei B, Jung J, Dwyer J (1996) Extensions of discontinuous deformation analysis for jointed rock masses. Int J Rock Mech Min Sci Geomech Abstr 33(7):671–694

Lisjak A, Tatone BSA, Grasselli G et al (2014) Numerical modelling of the anisotropic mechanical behaviour of opalinus clay at the laboratory-scale using fem/dem. Rock Mech Rock Eng 47(1):187–206

MacLaughlin MM, Doolin DM (2006) Review of validation of the discontinuous deformation analysis (DDA) method. Int J Numer Anal Meth Geomech 30:271–305

Mahabadi OK, Cottrell BE, Grasselli G (2010) An example of realistic modelling of rock dynamics problems: FEM/DEM simulation of dynamic Brazilian test on Barre granite. Rock Mech Rock Eng 43(6):707–716

Munjiza A (2004) The combined finite-discrete element method. Wiley, New York

Munjiza A, Andrews KRF (2000) Penalty function method for combined finite–discrete element systems comprising large number of separate bodies. Int J Numer Meth Eng 49:1377–1396

Rabczuk T, Belytschko T (2004) Cracking particles: a simplified meshfree method for arbitrary evolving cracks. Int J Numer Meth Eng 61(13):2316–2343

Shi GH (1988) Discontinuous deformation analysis—a new numerical model for the statics and dynamics of block systems. PhD Dissertation, Department of civil engineering, University of California, Berkeley.

Tsesarsky Y, Hatzor YH (2006) Tunnel roof deflection in blocky rock masses as a function of joint spacing and friction—a parametric study using discontinuous deformation analysis (DDA). Tunn Undergr Space Technol 21(1):29–45

Wang X, Li H, Wu W, Zhu H, Liu F, Zhang H (2021) Research progress of contact detection and cloud computing for 3D parallel explicit discontinuous deformation analysis. Hazard Control in Tunn Undergr Eng 3(3):111–118

Wu JH (2007) Applying discontinuous deformation analysis to assess the constrained area of the unstable Chiu-fen-erh-shan landslide slope. Int J Numer Anal Meth Geomech 31(5):649–666

Wu WA, Yang YT, Zheng H (2020a) Hydro-mechanical simulation of saturated and semi-saturated porous soil-rock mixtures using the numerical manifold method. Comput Meth Appl Mech Eng 370:113238.

Wu WA, Yang YT, Zheng H (2020b) Enriched mixed numerical manifold formulation with continuous nodal gradients for dynamics of fractured poroelasticity. App Math Model 86:225–258

Wu WA, Yang YT, Zheng H, Zhang LM, Zhang N (2022) Numerical manifold computational homogenization for hydro-dynamic analysis of discontinuous heterogeneous porous media. Comput Meth App Mech Eng 388:114254

Xu DD, Wu AQ, Yang YT, Lu B, Liu F, Zheng H (2020) A new contact potential based three-dimensional discontinuous deformation analysis method. Int J Rock Mech Min Sci 127:104206

Yan C, Jiao YY, Zheng H (2018) A fully coupled three-dimensional hydro-mechanical finite discrete element approach with real porous seepage for simulating 3D hydraulic fracturing. Comput Geotech 96:73–89

Yang YT, Xu DD, Zheng H (2018a) Explicit discontinuous deformation analysis method with lumped mass matrix for highly discrete block system. Int J Geomech 18(9):04018098

Yang YT, Tang XH, Zheng H, Liu QS, Liu ZJ (2018b) Hydraulic fracturing modeling using the enriched numerical manifold method. App Math Model 53:462–486

Yang YT, Sun GH, Zheng H, Yi Q (2019) Investigation of the sequential excavation of a soil-rock-mixture slope using the numerical manifold method. Eng Geo 256:93–109

Yang YT, Xu DD, Liu F, Zheng H (2020a) Modeling the entire progressive failure process of rock slopes using a strength-based criterion. Comput Geotech 126:103726

Yang YT, Sun GH, Zheng H, Yan CZ (2020b) An improved numerical manifold method with multiple layers of mathematical cover systems for the stability analysis of soil-rock-mixture slopes. Eng Geol 264:105373

Yang YT, Wu WA, Zheng H (2021a) An Uzawa-type augmented Lagrangian numerical manifold method for frictional discontinuities in rock masses. Int J Rock Mech Min Sci 148:104970.

Yang YT, Xia Y, Zheng H, Liu ZJ (2021b) Investigation of rock slope stability using a 3D nonlinear strength-reduction numerical manifold method. Eng Geol 292:106285

Yang YT, Wu WA, Zheng H (2023) Investigation of slope stability based on strength-reduction-based numerical manifold method and generalized plastic strain. Int J Rock Mech Min Sci 164:105358

Yeung MR, Jiang QH, Sun N (2003) Validation of block theory and three-dimensional discontinuous deformation analysis as wedge stability analysis methods. Int J Rock Mech Min Sci 40(2):265–275

Yeung MR, Sun N, Jiang QH, Blair SC (2004) Analysis of large block test data using three-dimensional discontinuous deformation analysis. Int J Rock Mech Min Sci 41(3):458–459

Yeung MR, Jiang QH, Sun N (2007) A model of edge-to-edge contact for three-dimensional discontinuous deformation analysis. Comput Geotech 34(2):175–186

Zhang H, Liu S, Chen G (2016) Extension of three-dimensional discontinuous deformation analysis to frictional-cohesive materials. Int J Rock Mech Min Sci 86:65–79

Zhao GF, Lian JJ, Russell AR, Zhao J (2017) Three-dimensional DDA and DLSM coupled approach for rock cutting and rock penetration. Int J Geomech 17(5):E4016015

Zhao L, Liu X, Mao J, Xu D, Munjiza A, Avital E (2018) A novel contact algorithm based on a distance potential function for the 3D discrete-element method. Rock Mech Rock Eng 51(12):3737–3769

Zheng F, Zhuang XY, Zheng H, Jiao YY, Rabczuk T (2020) Kinetic analysis of polyhedral block system using an improved potential-based penalty function approach for explicit discontinuous deformation analysis. Appl Math Model 82:314–335

Zhuang X, Augarde CE, Mathisen KM (2012) Fracture modeling using meshless methods and level sets in 3D: framework and modeling. Int J Numer Meth Eng 92:969–998

Zienkiewicz OC, Taylor RL (2000) The finite element method, 5th edn. Butterworth-Heinemann, Oxford